A Single Particle Model to Predict the Impact of Induced Condensing Agents on Polymerizing Particles During the Gas Phase Polymerization of Ethylene

Amel Ben Mrad, Nida Sheibat-Othman, Timothy Mckenna

A Single Particle Model to Predict the Impact of Induced Condensing Agents on Polymerizing Particles during the Gas Phase Polymerization of Ethylene

Amel Ben Mrad[a], Nida Sheibat-Othman[b], Timothy F. L. McKenna[a,*]

[a] CP2M, UCBL/CNRS-CPE, UMR 5265, Villeurbanne, France

[b] University of Lyon, University Claude Bernard Lyon 1, CNRS, LAGEPP UMR 5007, F-69100 Villeurbanne, France

Abstract

A single particle model for homopolymerization of ethylene in presence of hydrogen is used to predict the impact of induced condensing agents on the evolution of concentration profiles in the growing particle, the rate of homopolymerization and the evolution of the molecular weight distribution. The model formulation is based on the random-pore polymer flow model associated with a kinetic model using the method of moments to describe the chain length. The Sanchez-Lacombe equation of state is applied to calculate the equilibrium concentration of each penetrant in a mixture of gases in the amorphous polymer phase. The free volume model from Vrentas and Duda is employed to calculate the diffusivity coefficients of penetrants in a semi-crystalline polymer. The model confirms that the increased rates of production and increased molecular weights observed in previously published experimental studies are due in large part to the co-solubility and co-diffusivity effects.

Key words: Single particle model, polyethylene, induced condensing agents, co-solubility, co-diffusion, polymerization rate, molecular weight distribution

*E-mail address: timothy.mckenna@univ-lyon1.fr (T.F.L. McKenna)

Introduction

A growing polymer particle can be thought of as a dynamically evolving microreactor, which exchanges heat and matter with the continuous phase of the main reactor, and in which the polymer is formed. Upon injection into a reactor, the polymer particle will change rapidly, first by undergoing fragmentation, and then growing by expansion[1–4]. The rate at which this expansion occurs is linked to the rate of production of polymer, and thus to both the intrinsic activity of the used catalyst, and to the concentration of reactive species and the local temperature at the active sites; the same is true for the molecular weight[5]. The monomer concentration at an active site will be a trade-off between the rate at which it is consumed at a given point in the particle, and the rate at which it diffuses through the particle. During ethylene polymerization, monomer diffuses from the gas phase of the reactor into the pores of the supported particle, where it sorbs in the polymer covering the sites, then diffuses through the amorphous phase to the active sites. Heat is produced when the monomer reacts at the active site, and this heat must be transported out of the particle to avoid overheating. Thus, to describe the polymerization reaction in terms of reaction rate and polymer properties, it is imperative to be able to predict the dynamics of mass and heat transfer in the growing particle.

Most modelling studies now employ a version of the polymer flow model (PFM)[6–8] to describe particle growth and estimate the concentration and temperature gradients (i.e. as a single particle model – SPM). These models assume that transport is by Fickian diffusion. The choice of which model to use has been extensively discussed in the literature[2,5,9–11], so interested readers may refer to these references for further information. In the current work we choose to use the Random Pore Polymer Flow Model (RPPFM) to describe the single particle behavior since it combines a certain amount of geometric simplicity with a mechanistic description of the diffusion process[12]. This model takes into account the average transport phenomena through the pore phase and the mass transfer through the semicrystalline polymer phase. Of course, like all other SPM, it has its limitations. We cannot use it to predict the evolution of the particle morphology, so it is needed to make assumptions about the porosity. Furthermore, we still do not know how to predict parameters such as the rate of crystallization of the polymer, so it is difficult to account for such changes that risk being important during the initial phases of reaction. Nevertheless, with the appropriate assumptions, the RPPFM can certainly be used to capture the main tendencies in terms of the impact of process parameters

on the polymerization rate in a better way than other models assuming thermodynamic equilibrium.

Turning to reactor technology, at the time this article is written fluidized bed reactors (FBRs) are the only type gas phase reactors used to make PE commercially because they run with relative gas-particle velocities that are higher than those typically found in other gas phase reactors. This is essential because of the heat generated by the highly exothermic ethylene polymerization, and the poor heat capacity of gas phase systems. Heat removal is one of the major challenges in olefin polymerization from a process engineering point of view, and is the limiting factor in the race to increase production rates[13]. In order to optimize the productivity, condensed mode cooling is employed in order to increase the capacity of heat removal. In condensed mode operation, in addition to injecting ethylene, hydrogen, and eventually a comonomer, inert alkanes as such as propane, isobutane, n-pentane or n-hexane, are used to increase the heat capacity of the gas phase in the reactor, and if fed in liquefied form, they also provide a latent heat of vaporization that increases the energy absorption in the reactor[9,13–16]. These compounds are often referred to as induced condensing agents (ICA). The interested reader is referred to reference[13] for a more in-depth discussion of the choice and impact of ICA on gas phase PE production. However, one thing that occurs when an inert ICA is added to the polymerization reactor is very important and verifiable: recent experimental papers from our group have shown that the reaction rate and the molecular weight increase in the presence of ICA, despite the fact that these compounds are chemically inert[13,14,17–21]. These observations are attributed to the fact that an ICA exhibits a "co-solubility effect" on the ethylene solubility in the amorphous phase of the polymers covering the active sites. However, the co-solubility effect alone could not explain the increase in the reaction rate and therefore it would be quite useful to adapt a single particle model of gas phase ethylene polymerization that can help explain and predict these effects.

In that sense, Alizadeh et al.[22] extended the work of Kanellopoulos et al.[12] to include an accurate thermodynamic description through the Sanchez-Lacombe EoS as sorption model and Vrentas and Duda[23,24] as diffusion model. They suggested that combined co-solubility and co-diffusion effects had a noticeable impact on the mass and heat transfer, as well as on the polymerization rate. They used the SL EoS model to account for the co-solubility effects with n-hexane, but did not try to link the reaction rate to the polymer molecular weight data.

In this paper, a comprehensive SPM, accounting for mass and heat transfer limitations appearing during the early growth of a Ziegler-Natta catalyst in gas phase olefin

polymerization is developed. The RPPFM model will be adapted in order to predict the temporal-spatial evolution of concentration of the different species (i.e. monomer, ICA, live and dead polymer chains) and temperature profiles in the growing polymer particle and so to estimate the overall particle polymerization rate and the evolution of molecular weight distribution. However, the accurate determination of both the penetrants concentration at the catalyst active site and the effective penetrant diffusion coefficient is crucial in any particle growth modeling study. This study will therefore show the importance of having an accurate thermodynamic model when developing a particle growth model. The Sanchez-Lacombe EoS for multicomponent systems (i.e. monomer, penetrants), as thermodynamic model, is incorporated in this particle model, in order to calculate the equilibrium concentration of penetrants in the amorphous phase of the polymer. The Vrentas and Duda diffusivity model is applied to calculate the diffusivity of penetrant molecules in the semicrystalline polymer. Finally, a kinetic model for homopolymerization is included to predict the changes in the polymer molecular weight in the growing particle as a function of the gas phase composition.

Model Development

Single Particle Model - RPPFM

In the present study, the Random-Pore Polymer Flow Model (RPPFM)[12,25] has been adapted to predict the spatial-temporal evolution of monomer and ICA concentrations, temperature, polymerization rate and polymer molecular weight in gas-phase ethylene polymerization. For the purposes of modelling, the following assumptions have been made:

- The particle is assumed to be spherical;
- The particle is considered to be a pseudo-homogeneous medium, with an average porosity, and with the active sites uniformly dispersed throughout the particle;
- The fragmentation process is completed instantaneously;
- The crystallinity as well as the porosity of the produced polymer are assumed to be constant during the reaction;
- The hydrogen concentration in the polymer is very low compared to the other penetrants (i.e. ethylene, n-pentane) and is therefore assumed constant and unaffected by the presence of an ICA.

These assumptions simplify the numerical calculations, but as discussed in the literature[2,5,9–11], a good number of them are not entirely true. We know that the morphology of the particles

evolves rapidly during the first minutes of the polymerization. During this time, the crystallinity, critical length scale for diffusion, and perhaps even the number and nature of the active sites also change. Furthermore, it is possible that the relatively high ICA concentrations with respect to polymer during the initial phases of the reaction can retard crystallization, which in turn could have an impact on the diffusion of monomer to the active sites. Moreover, swelling of the amorphous phase by a penetrant might not be uniform in the whole particle, as it can be affected by the tie molecules.[26] As the main purpose of this paper is to quantify the impact of the gas phase composition (i.e. monomer, ICA, hydrogen) on the reaction rate and molecular weight distributions, we will not attempt to model the nascent phase of the polymerization. Rather, we choose to fit the kinetic parameters (see below) to the experimental data after 5 minutes of the polymerization. This will allow us to calculate the mass and heat transfer in the growing polymer particle for a long time, therefore, to approximate the impact of the ICA on the rate and molecular weight data reasonably well.

The full set of mass and energy balances used within the RPPFM framework and the corresponding initial and boundary conditions are presented in Table 1.

Table 1. Material and energy balance with initial and boundary conditions of the single particle model.

	Initial condition	**Boundary conditions**
Ethylene mass balance:		
$\frac{\partial[M_1]}{\partial t} = \frac{1}{r^2}\frac{\partial}{\partial r}\left(D_{1,\mathrm{ov}} r^2 \frac{\partial[M_1]}{\partial r}\right) - R_{\mathrm{v}}$	$[M_1]_{(r,0)} = 0$	$[M_1]_{(R,t)} = [M_1]^{\mathrm{eq}}$ $\frac{\partial[M_1]_{(0,t)}}{\partial r} = 0$
ICA mass balance:		
$\frac{\partial[M_2]}{\partial t} = \frac{1}{r^2}\frac{\partial}{\partial r}\left(D_{2,\mathrm{ov}} r^2 \frac{\partial[M_2]}{\partial r}\right)$	$[M_2]_{(r,0)} = 0$	$[M_2]_{(R,t)} = [M_2]^{\mathrm{eq}}$ $\frac{\partial[M_2]_{(0,t)}}{\partial r} = 0$
Energy balance:		
$\rho_{\mathrm{ov}} C_{\mathrm{p,ov}} \frac{\partial T}{\partial t} = \frac{k_{\mathrm{c,p}}}{r^2}\frac{\partial}{\partial r}\left(r^2 \frac{\partial T}{\partial r}\right) + \left(-\Delta H_{\mathrm{p}}\right) R_{\mathrm{v}}$	$T_{(r,0)} = T_{\mathrm{b}}$	$-k_{\mathrm{c,p}} \frac{\partial T_{(R,t)}}{\partial r} = h(T - T_{\mathrm{b}})$ $\frac{\partial T_{(0,t)}}{\partial r} = 0$

In Table 1, t and r represent the time and radial position inside the particle, respectively. R is the radius of the pseudohomogeneous particle at each moment during its growth. $D_{i,\mathrm{ov}}$ is the overall diffusion coefficient of penetrant molecule i in the polymeric particle, $[M_i]$ is the overall concentration of penetrant i and $[M_i]^{\mathrm{eq}}$ is the overall equilibrium concentration of the same species in the amorphous phase of the polymer calculated with the Sanchez-Lacombe EoS, $i = 1$ for ethylene and $i = 2$ for the ICA. In the energy balance, T, ΔH_{p}, $k_{\mathrm{c,p}}$, $C_{\mathrm{p,ov}}$ and ρ_{ov}

represent respectively the temperature, the enthalpy of ethylene polymerization $\Delta H_{\mathrm{p}} = -107.5$ kJ mol^{-1}, the thermal conductivity of the polymer phase $k_{\mathrm{c,p}} = 0.2$ J (m.s.K)$^{-1}$, the heat capacity of the particle $C_{\mathrm{p,ov}} = \left([M_1]MW_1C_{p1} + [M_2]MW_2C_{p2} + \rho_{\mathrm{p}}C_{p,\mathrm{pol}}\right)/\rho_{\mathrm{ov}}$, and the overall particle density $\rho_{\mathrm{ov}} = [M_1]MW_1 + [M_2]MW_2 + \rho_{\mathrm{p}}(1-\varepsilon)$ where ρ_{p} is the density of the polymer phase,. In the boundary condition, h and T_{b} are the heat transfer coefficient of the particle and the bulk temperature of the reactor, respectively. The use of the Ranz-Marshall correlation for the calculation of the external film heat transfer coefficient has been critically examined, and it can result in an overestimation of the particle temperature[12]. Nevertheless, we will use it here as the polymerization rates of the experiments serving as a basis for the estimation of the model parameters are moderate, so no large temperature excursions are expected.

Thermodynamics: Sanchez-Lacombe Equation of State

A number of papers have shown that Henry law is not applicable to polymer-penetrant systems involving heavy penetrants vapors and high pressures, nor to multicomponent systems where a co-solubility effect may exist[27,28]. It is therefore essential to use a more sophisticated thermodynamic model to obtain a realistic description of the system, to better describe the interactions between the different penetrants and the polymer. In the present study, the Sanchez-Lacombe equation of state (SL EoS) is employed to calculate the equilibrium concentration of the different species (i.e. monomer and ICA) in the amorphous phase of the polymer. SL EoS is a lattice-fluid model in which pure components are assumed to be broken into parts and placed into a lattice structure. The SL EoS introduces the concept of vacant lattice sites or holes to account for the compressibility and the density changes. Thus, the system volume or density can vary by changing the fraction of holes in the lattice structure[29]. The main equation of state is given by:

$$\bar{\rho}^2 + \bar{P} + \bar{T}\left[\ln(1-\bar{\rho}) + \left(1 - \frac{1}{r}\right)\bar{\rho}\right] = 0 \qquad (1)$$

where $\bar{T} = T/T^*$, $\bar{P} = P/P^*$ and $\bar{\rho} = \rho/\rho^*$ are the reduced temperature, pressure, and density respectively. T^*, P^*, and ρ^* are the scale factors known as the characteristic temperature, pressure, and density respectively, which are used to characterize each pure component in the mixture(

Table 2). The development of SL EoS has been described in references[30,31], so will not be described here.

Table 2. Pure component parameters used in SL EoS.

Component	T^* (K)	P^* (bar)	ρ^* (kg m^{-3})	Reference
Ethylene	283	3395	680	[32]
n-pentane	445	3060	755	[32]
n-hexane	476	2979.1	775	[22]
LLDPE	653	4360	903	[32]

The only adjustable parameters in the SL EoS are the interaction parameters between the different species in the mixture, k_{ij}. We believe that the interaction parameters between small molecules are equal to zero, which leaves us the interaction parameters between vapor species and the polymer to be identified. (1) represents ethylene, (2) the ICA and (3) the polymer, meaning that k_{13} and k_{23} are the only adjustable parameters for ternary systems. The interaction parameters for ethylene/n-hexane/LLDPE were taken from Alizadeh et al.[22] and the ones for ethylene/n-pentane/LLDPE were identified by fitting SL EoS to experimental solubility data from Yao et al.[33]. They measured experimentally the solubility of ethylene/n-pentane in semi-crystalline LLDPE of crystallinity of 48.6 % at temperatures between 70-90 °C and a total pressure of 20 bar with n-pentane partial pressure of 0.8-1.8 bar. These identified k_{ij} can therefore be used in the present particle model since the PE used as a reference to validate the model has a crystallinity of 45 %, and n-pentane partial pressure are between 1-2 bar which are close to the experimental conditions of Yao et al.[33]. k_{ij} used in the different simulations are given in Table 3.

The equilibrium concentrations of the different species in the semicrystalline polymer calculated from SL EoS for ternary systems have been incorporated in the RPPFM model as boundary conditions of the material balances.

Table 3. Binary and ternary interaction parameters of ethylene/n-pentane/LLDPE system from Sanchez-Lacombe EoS at 80°C.

System	k_{ij}	Reference
Ethylene/LLDPE	k_{13} = -0.022	[34]
n-pentane/LLDPE	k_{13} = 0.024	[34]
n-hexane/LLDPE	k_{13} = 0.010	[22]
Ethylene/n-pentane/LLDPE	k_{13} = -0.027, k_{23} = 0.0501	[33]
Ethylene/n-hexane/LLDPE	k_{13} = -0.022, k_{23} = 0.029	[22]

Since the solubility of hydrogen in the amorphous phase of the polymer is quite low compared to that of ethylene or n-pentane, the presence of hydrogen is assumed to have no effect on the solubility or diffusivity of ethylene in the particle model (and vice versa). The concentration of hydrogen, calculated with Henry's law, is therefore assumed to be constant in the whole particle over time, and not influencing the concentration/diffusion of ethylene:[35]

$$[H_2] = k_{\mathrm{He,H_2}} P_{\mathrm{H_2}} \frac{\rho_{\mathrm{p}}}{MW_{\mathrm{H_2}}} \quad (2)$$

with $k_{\mathrm{He,H_2}} = 8.2533 \times 10^{-5}$ g Pa^{-1} g^{-1} amorphous polymer.

Vrentas and Duda Diffusion Model

The knowledge of the overall diffusion coefficient is important in the material balances of the RPPFM to allow us to describe the diffusion of species from the bulk phase to the catalyst active sites through the pores and the amorphous polymer. A convenient way to do this is to use the random-pore model proposed by Wakao and Smith[36], and adapted by Kanellopoulos et al.[25] and Yiagolopoulos et al.[37] for olefin polymerization. The effective (or overall) diffusion coefficient depends not only on the temperature and concentration of the penetrants in the amorphous phase of the polymer, but also on the particle porosity (ε). Based on these works, the overall diffusion coefficient of species i can be expressed as follows:

$$D_{i,\mathrm{ov}} = \frac{\varepsilon}{\tau_{\mathrm{f}}^2} D_{i,\mathrm{g}} + (1-\varepsilon)(1+3\varepsilon) D_{i,\mathrm{pol}} \quad (3)$$

in which τ_{f} denotes the tortuosity factor of the pore phase of the particle. Its value is assumed to be equal to 10[22,25]. The first term on the right-hand side of this equation represents the transport of the penetrants through the pores while the second term accounts for mass transfer through the semicrystalline polymer phase. The diffusion in the porous polymer particle is calculated by Chapman-Enskog correlation, and details on calculating this can be found elsewhere[37]. $D_{i,\mathrm{pol}} = D_{i,\mathrm{am}}^{\mathrm{ter}}/(\tau\beta_i)$, with β_i the chain immobilization factor accounting for the reduction in amorphous chain segmental mobility due to the proximity of crystallites and τ denotes the tortuosity factor corresponding to the magnitude of extension in the diffusion path associated with bypassing impermeable crystallites by the penetrant[22]. The diffusion of small molecules in the semicrystalline polymer has been studied extensively and has shown that the free volume theory refined by Vrentas and Duda[23,38,39] correlates accurately the diffusion coefficient at various temperatures and over a large concentration range. According to the free-volume theory[24], the diffusion coefficient of ethylene (1) and an ICA (2) in the amorphous PE (3) in the ternary system is given by:

$$D_{1,\mathrm{am}}^{\mathrm{ter}} = D_{01}\exp\left(-\frac{\omega_1\hat{V}_1^* + \omega_2\hat{V}_2^*\xi_{13}/\xi_{23} + \omega_3\hat{V}_3^*\xi_{13}}{\omega_1\frac{K_{11}}{\gamma}(K_{21}+T-T_{\mathrm{g1}}) + \omega_2\frac{K_{12}}{\gamma}(K_{22}+T-T_{\mathrm{g2}}) + \omega_3\frac{K_{13}}{\gamma}(K_{23}+T-T_{\mathrm{g3}})}\right) \quad (4)$$

$$D_{2,\mathrm{am}}^{\mathrm{ter}} = D_{02}\exp\left(-\frac{\omega_2\hat{V}_2^* + \omega_1\hat{V}_1^*\xi_{23}/\xi_{13} + \omega_3\hat{V}_3^*\xi_{23}}{\omega_1\frac{K_{11}}{\gamma}(K_{21}+T-T_{\mathrm{g1}}) + \omega_2\frac{K_{12}}{\gamma}(K_{22}+T-T_{\mathrm{g2}}) + \omega_3\frac{K_{13}}{\gamma}(K_{23}+T-T_{\mathrm{g3}})}\right) \quad (5)$$

in which D_{0i} is the pre-exponential term for component i, ω_i its weight fraction in the amorphous polymer phase calculated from SL EoS, $\hat{V}_i^*$ its specific hole free volume required for a diffusion jump, K_{1i} and K_{2i} its free-volume parameters, $T_{\mathrm{g}i}$ its glass transition temperature of and γ is the overlap factor introduced because the same free volume is available for more than one molecule. Table 4 shows the free-volume theory parameters necessary for the studied systems.

Table 4. Parameters of the free-volume theory.

	Ethylene	***n*-pentane**	***n*-hexane**	**PE**	**Unit**
D_{0i}	2.96×10^{-7}	3.11×10^{-8}	3.50×10^{-8}	-	$m^2\ s^{-1}$
$\hat{V}_i^*$	1.341	1.158	1.133	1.006	$cm^3\ g^{-1}$
K_{1i}/γ	1.97×10^{-3}	2.41×10^{-3}	1.96×10^{-3}	1.02×10^{-3}	$cm^3\ g^{-1}\ K^{-1}$
$K_{2i} - T_{\mathrm{g}i}$	42.38	-38.89	-41.08	-228.70	K
MW_i	28.05	72.15	86.18	-	$g\ mol^{-1}$
ξ_{i3}	0.4548	0.9566	0.9184	-	(-)
References	[22,40]	[38]	[22]	[41]	

The ξ_{i3} parameter is the ratio of polymer and solvent molar jumping units[40], defined as follows:[32,38]

$$\xi_{i3} = \frac{\bar{V}_i^0(0)}{\bar{V}_{3j}^*} = \frac{MW_i * \hat{V}_i^*}{\bar{V}_{3j}^*} \quad (6)$$

Where $\bar{V}_i^0(0)$ is the penetrant molar volume at 0 K ($m^3\ mol^{-1}$), $\bar{V}_{3j}^*$ the critical molar volume of the polymer jumping unit *j* ($m^3\ mol^{-1}$) and MW_i is the molecular weight of penetrant *i*.

Number of Types of Active Sites: Deconvolution of the MWD

It is well accepted that Ziegler-Natta (ZN) catalysts are multi-site catalysts; in other words, each catalyst particle will contain a certain number of "families" of active sites. These families will propagate at different rates, insert comonomer at different rates and eventually respond to hydrogen differently. To identify the minimum number of "families" of active sites

needed to describe the behavior of a catalyst system, one can deconvolute the measured MWD.[42] A series of ethylene polymerizations in the presence of n-pentane and hydrogen over a commercial ZN catalyst was realized and the MWD of the final samples were measured (by Viscotek High-Temperature Triple Detection Gel Permeation Chromatography, HT-GPC), and the obtained MWD was deconvoluted. The used experimental conditions are given in Table 5 and the detailed experimental set-up is outlined in reference [22].

Table 5. Partial pressures of n-pentane and hydrogen for each polymerization experiment. All pressures are in bar. P_{C_2}=7 bar.

	R_{p1}	R_{p2}	R_{p3}	R_{p4}	R_{p5}
P_{C_5}	0	1	2	0	2
P_{H_2}	0			3	

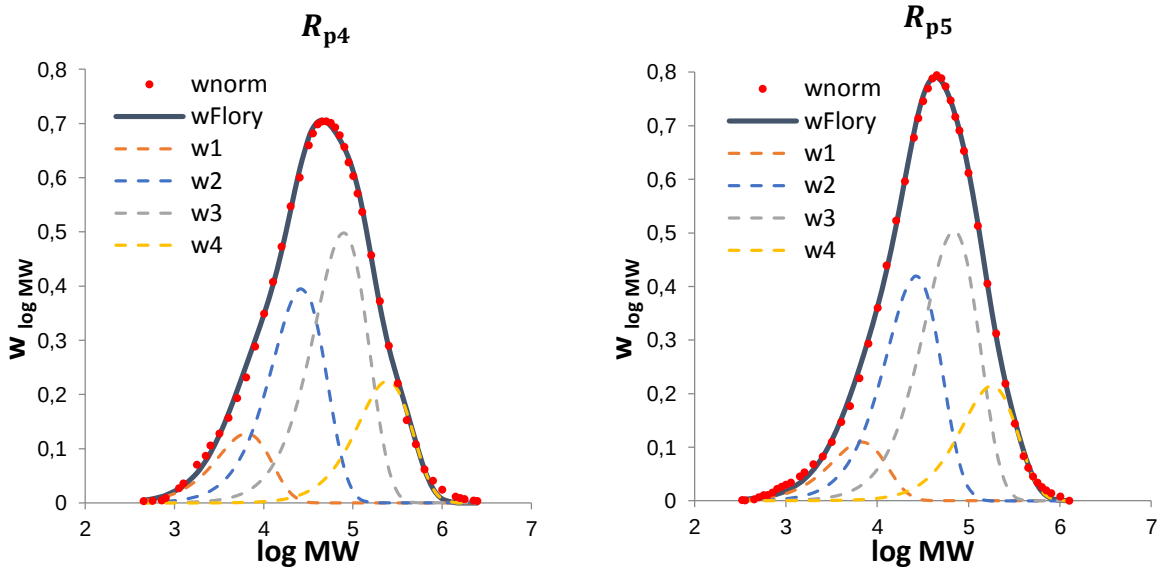

Figure 1. Deconvolution of the experimental MWD (red dots, w_{norm}) for R_{p_4} and R_{p_5} suggests that it is reasonable to use a minimum of 4 site types to describe this catalyst, designated by 1, 2, 3 and 4, respectively. w_{Flory} represents the global calculated MWD.

Table 6. Weight fraction of each catalyst active site obtained from the deconvolution.

	Site 1	Site 2	Site 3	Site 4
R_{p_4}	0.1	0.32	0.40	0.18
R_{p_5}	0.09	0.34	0.40	0.17
w_{m_k}	0.095	0.33	0.4	0.175

Figure 1 shows the experimental MWD and the results of the deconvolution. It appears from this analysis that the MWD can be adequately described with four distributions corresponding

to the four site types, for experiments R_{p4} and R_{p5}. Table 6 shows the weight fraction of each site type for each experiment separately, from which the average value of both experiments was calculated (w_{m_k}). These fractions will be used to identify the polymerization parameters by fitting the measured reaction rate and MWD to the experiments in the following sections. The initial concentration of each catalyst active sites is considered as follows:

$$C_{0,k}^{*} = w_{\mathrm{m}_k}\, C^{*} = w_{\mathrm{m}_k}\, f_{\mathrm{cat}} C_{\mathrm{max}}^{*} = w_{\mathrm{m}_k}\, f_{\mathrm{cat}} \frac{w_{\mathrm{Ti}} \rho_{\mathrm{cat}}}{MW_{\mathrm{Ti}}} \qquad (7)$$

Where C^{*} is the active site concentration, MW_{Ti} the molecular weight of titanium, ρ_{cat} the density of the catalyst and f_{cat} the efficiency factor of the catalyst. C_{max}^{*}, the concentration of metal sites for the $TiCl_4$ supported on MgCl2 Ziegler-Natta catalyst, was calculated using the mass fraction of Titanium in the catalyst, w_{Ti}. The used catalyst has w_{Ti}= 2.8 wt %.[43]

Kinetic Model and MWD

Following from the deconvolution analysis, a four-site kinetic model is employed in the present study to describe ethylene polymerization in multicomponent system (i.e. ethylene, n-pentane or n-hexane) over a Ziegler-Natta catalyst. The kinetic mechanism shown in Table 7 comprises a classic series of elementary reactions including initiation and propagation reactions, transfer to monomer, molecular weight control reactions (i.e. transfer to H_2, initiation of hydrogen bearing catalyst sites P_H^k) and a first order spontaneous deactivation reaction. We assume that site activation is instantaneous.

Table 7. Kinetic scheme of ethylene homopolymerization over a Ziegler-Natta 4 sites catalyst ($k = 1 - 4$).

Initiation	$C_k^{*} + M \xrightarrow{k_{\mathrm{i}}^k} P_r^k$
Propagation	$P_r^k + M \xrightarrow{k_{\mathrm{p}}^k} P_{r+1}^k$
Transfer to H_2	$P_r^k + H_2 \xrightarrow{k_{\mathrm{tH}}^k} P_{\mathrm{H}}^k + D_r^k$
Initiation of P_H	$P_H^k + M \xrightarrow{k_{\mathrm{iH}}^k} P_1^k$
Transfer to monomer	$P_r^k + M \xrightarrow{k_{\mathrm{tM}}^k} P_1^k + D_r^k$
Spontaneous chain transfer	$P_r^k \xrightarrow{k_{\mathrm{tsp}}^k} C_k^{*} + D_r^k$
Deactivation	$P_r^k \xrightarrow{k_{\mathrm{d}}^k} C_{\mathrm{d}}^k + D_r^k$

In Table 7, C_k^* is the concentration of vacant catalyst active sites, M the monomer concentration, P_r^k the concentration of live polymer chains of length r, P_H^k the concentration of the activated vacant catalyst sites occupied by a hydrogen, D_r^k the concentration of dead polymer chains, H_2 the hydrogen concentration and C_d^k is the concentration of deactivated catalyst site. The symbol k denotes the four catalyst active sites: 1, 2, 3 and 4. Based on the proposed kinetic scheme, the moments of live, μ_i^k, and dead, η_i^k, chain length distributions were calculated (Table 8).

Table 8. Local mass balances of active sites and moments of chain lengths, with the initial conditions: $\mu_i^k(r,0) = \eta_i^k(r,0) = 0$, $P_H^k(r,0) = 0$, $C_k^*(r,0) = C_{0,k}^*$, $i = 0,1,2$, $k = 1,2,3,4$.

0th moment of living chains	$\boldsymbol{\frac{d\mu_0^k}{dt} = \left(k_i^k C_k^* + k_{iH}^k P_H^k\right)[M] - \left(k_{tH}^k[H_2] + k_d^k + k_{tsp}^k\right)\mu_0^k}$
1st moment of living chains	$\frac{d\mu_1^k}{dt} = \left(k_i^k C_k^* + k_{iH}^k P_H^k + \left(k_p^k + k_{tM}^k\right)\mu_0^k\right)[M] - \left(k_{tH}^k[H_2] + k_d^k + k_{tM}^k[M] + k_{tsp}^k\right)\mu_1^k$
2nd moment of living chains	$\frac{d\mu_2^k}{dt} = \left(k_i^k C_k^* + k_p^k\left(2\mu_1^k + \mu_0^k\right) + k_{iH}^k P_H^k + k_{tM}^k\mu_0^k\right)[M] - \left(k_{tH}^k[H_2] + k_d^k + k_{tM}^k[M] + k_{tsp}^k\right)\mu_2^k$
0th moment of dead chains	$\frac{d\eta_0^k}{dt} = \left(k_{tH}^k[H_2] + k_d^k + k_{tM}^k[M] + k_{tsp}^k\right)\mu_0^k$
1st moment of dead chains	$\frac{d\eta_1^k}{dt} = \left(k_{tH}^k[H_2] + k_d^k + k_{tM}^k[M] + k_{tsp}^k\right)\mu_1^k$
2nd moment of dead chains	$\frac{d\eta_2^k}{dt} = \left(k_{tH}^k[H_2] + k_d^k + k_{tM}^k[M] + k_{tsp}^k\right)\mu_2^k$
Active sites	$\frac{dC_k^*}{dt} = k_{tsp}^k\mu_0^k - \left(k_i^k[M] + k_d^k\right)C_k^*$
Catalyst sites bearing hydrogen, $\boldsymbol{P_H^k}$	$\frac{dP_H^k}{dt} = k_{tH}^k\,\mu_0^k[H_2] - k_{iH}^k P_H^k[M] - k_d^k P_H^k$

The total polymerization rate of ethylene (per volume of catalyst) is given by:

$$R_p(r,t) = \sum_{k=1}^{N_s} k_p^k \mu_0^k [M_1] \tag{8}$$

where N_s is the number of catalyst site types.

The average reaction rate over the particle is given by (used to compared to experimental data):

$$R_{p,ov}(t) = \frac{\int R_p(r,t)\,dv}{v} \tag{9}$$

The polymerization rate per polymer volume is calculated by:

$$R_{\mathrm{v}} = R_{\mathrm{p}}\left(\frac{1-\epsilon}{\varphi^3}\right) \tag{10}$$

where φ is the overall growth factor defined as $\varphi = R_{\mathrm{pol}}/r_{\mathrm{cat}}$. Where v is the particle volume.

The model equations were solved using the function pdepe of Matlab®. All the material balances (and the required variables such as the diffusion coefficients) were calculated locally as a function of the resulting concentrations and temperature (radially and over time). So, the coupling is ensured at each instance for all variables. A time loop is considered where the model is simulated for 40 seconds and the resulting reaction rate is used to calculate the volume of polymer produced, and so the new radius, to update the grid:

$$\frac{\mathrm{d}R_{\mathrm{pol}}}{\mathrm{d}t} = \frac{R_{\mathrm{v,ov}}\, R_{\mathrm{pol}}\, \mathrm{MW}_1}{3\rho_{\mathrm{ov}}} \tag{11}$$

where R_{pol} is the equivalent radius of the polymer-only particle at each time step during the reaction, initialized at r_{cat}, the radius of initial catalyst particle. The particle radius, used as a grid to simulate the model, is given by $R = R_{\mathrm{pol}}/(1-\epsilon)^{1/3}$.

All the rate constants are described by the Arrhenius law as follow:

$$k = k_0 \exp\left(-\frac{E_{\mathrm{a}}}{RT}\right) \tag{12}$$

in which T, E_{a} and R are the temperature, the activation energy and the universal gas constant, respectively.

The cumulative number average molecular weight of the polymer:

$$\bar{M}_{\mathrm{n}}(r,t) = \frac{\sum_{k=1}^{N_{\mathrm{s}}}(\mu_1^k+\eta_1^k)}{\sum_{k=1}^{N_{\mathrm{s}}}(\mu_0^k+\eta_0^k)} MW_1 \tag{13}$$

The cumulative weight average molecular weight of the polymer:

$$\bar{M}_{\mathrm{w}}(r,t) = \frac{\sum_{k=1}^{N_{\mathrm{s}}}(\mu_2^k+\eta_2^k)}{\sum_{k=1}^{N_{\mathrm{s}}}(\mu_1^k+\eta_1^k)} MW_1 \tag{14}$$

The MWD was reconstructed from these average values assuming that each catalyst site type produces a polymer where the chain lengths follow a lognormal distribution:

$$w(k, M_{\mathrm{w}}) = \frac{1}{M_{\mathrm{w}}\sigma_{\ln}(k)\sqrt{2\pi}} \exp\left(-\frac{\left(\ln M_{\mathrm{w}} - \ln \bar{M}_{\mathrm{n,ov}}(k)\right)^2}{2\sigma_{\ln}^2(k)}\right) \tag{15}$$

Where M_{w} is the polymer molecular weight, the variance is $\sigma_{\ln}(k) = \sqrt{\ln \frac{\bar{M}_{\mathrm{w,ov}}(k)}{\bar{M}_{\mathrm{n,ov}}(k)}}$, $w(k, M_{\mathrm{w}})$ is a density distribution as a function of $\ln M_{\mathrm{w}}$, and $\bar{M}_{\mathrm{n,ov}}(k)$ is the average value of $\bar{M}_{\mathrm{n}}(r,t)$ over the whole particle. The total MWD is then the sum of the MWD produced by the different catalyst sites, which is then normalized and transformed to a molar mass density to permit comparison with the experimental MWD given from the HT-GPC:

$$w_{\mathrm{tot}}(t, M_{\mathrm{w}}) = M_w \sum_{k=1}^{4} \frac{w(k,M_{\mathrm{w}}) w_{\mathrm{m}_k}}{\int_0^{\infty} w(k,M_{\mathrm{w}}) \mathrm{d}M_{\mathrm{w}}} \tag{16}$$

Parameter Identification

The measured polymerization rate with time, and the measured final polymer MWD have been fitted to the model in order to identify a set of representative kinetic parameters, using the following minimization criterion:

$$J = \frac{|\bar{m}_{\mathrm{w,m}} - \bar{m}_{\mathrm{w,exp}}|}{\bar{m}_{\mathrm{w,exp}}} + \sum_{t=5,10,15,20\ \mathrm{min}} \frac{|R_{\mathrm{p}}(t) - R_{\mathrm{p}}^{\mathrm{exp}}(t)|}{R_{\mathrm{p}}^{\mathrm{exp}}(t)} \tag{17}$$

Where $\bar{m}_{\mathrm{w,m}}$ and $\bar{m}_{\mathrm{w,exp}}$ are the modes of the final model MWD, $w_{\mathrm{tot}}(M_{\mathrm{w}})$, and experimental $w_{\mathrm{logM_w}}^{\mathrm{exp}}(M_{\mathrm{w}})$, respectively.

Some parameters were taken from literature, such as the rate constants of transfer to monomer, k_{tm0}, spontaneous termination, k_{tsp0}, as well as the activation energy of the different constants, E_{a} =37656 J mol^{-1} for initiation, reinitiation, propagation, and E_{a} =33472 J mol^{-1} for transfer and deactivation reactions[44]. The parameter k_{iH0} was considered to be equal to k_{i0}, as was assumed by McAuley et al. for instance[46]. For the sake of simplicity, the kinetic parameters were taken the same for all catalyst site types, except for transfer to hydrogen, k_{tH0}. In order to be able to predict the experimental width of the MWD, it was found that the transfer to hydrogen parameters of the different active sites can be related as follows: $k_{\mathrm{tH0}}^1 = 8k_{\mathrm{tH0}}^4$, $k_{\mathrm{tH0}}^2 = 6k_{\mathrm{tH0}}^4$ and $k_{\mathrm{tH0}}^3 = 4k_{\mathrm{tH0}}^4$. Once again, the goal of this modelling study is to show realistic values of the impact of the ICA on the polymerization process, and not to model the reaction accurately for this catalyst. These parameters give us however a reasonable approximation of ZN kinetics so that the thermodynamic effects can be highlighted independently.

Table 9. Values of the kinetic parameters used for the model of ethylene polymerization in gas-phase. The same parameters are used for all sites, except transfer to hydrogen ([a] the given value is for catalyst site type n° 4).

	Pre-exponential factor	Reference
Initiation	*94	This work
Reinitiation of sites bearing hydrogen	*94	This work
Propagation	*1.4×10^{6}	This work
Transfer to H_2	*20.6 [a]	This work
Transfer to monomer	*0.186	[44]
Spontaneous chain transfer	**8.84	[44,45]
Deactivation	**33	This work

***(m^3 mol^{-1} s^{-1}), ** (s^{-1})**

This leaves us with 5 parameters that need to be identified by fitting the model to experimental data: k_{i0}, k_{p0}, k_{d0}, k_{tH0}^{4} and f_{cat}. In order to do so, the experiments without hydrogen were first fitted to the model in order to identify k_{i0}, k_{p0}, k_{d0} and f_{cat}. The parameters k_{p0} and f_{cat} were used to adjust the level of R_{p} during the entire period of the reaction, while k_{i0} was used to tune the initial amplitude of R_{p} and k_{d0} was used to adapt the slope of R_{p}. Then, the experiments with hydrogen were fitted by keeping the previously identified parameters constant, and by changing only k_{tH0}^{4} which serves to adjust the MWD and R_{p}. Some adjustment of k_{p0} and f_{cat} were needed when fitting to experiments with hydrogen. Indeed, these two parameters have the same impact on the reaction rate, and so they might not be identifiable based on the measurement of R_{p} alone. However, they do not have the same impact on the molecular weight (as f_{cat} does not influence the polymer molecular weight), therefore using both measurements can improve their identification. The adjusted value of f_{cat} was found to be 0.9, and the other parameters can be found in Table 9.

Figure 2 compares the experimental and modelling results of the reaction rate, in presence of different amounts of pentane, in the absence of hydrogen. Figure 3 and 4, compare the experimental and modelling results of the reaction rate and the MWD, obtained in the presence of 3 bar of hydrogen. These results show that the predicted model and the experimental reaction rates and MWDs are acceptably in agreement at different compositions of the gas phase (i.e. n-pentane, hydrogen). The model can capture well the effect of n-pentane (as ICA) and hydrogen on the reaction rate and MWD. The model does not fit the initial rate of polymerization particularly well, and this point has been discussed in reference [22]. There are a number of effects which are not included in the discussion here, including the possible evolution of the crystallinity, changes of particle morphology and possible overheating during the initial stages that might cause the initial rate to be higher than that predicted. As our goal is to demonstrate the importance of understanding and incorporating

the cosolubility effect, there was no need to complicate the model (and it is far from clear how to include certain effects such as changing porosity and the dynamics of polymer crystallization).

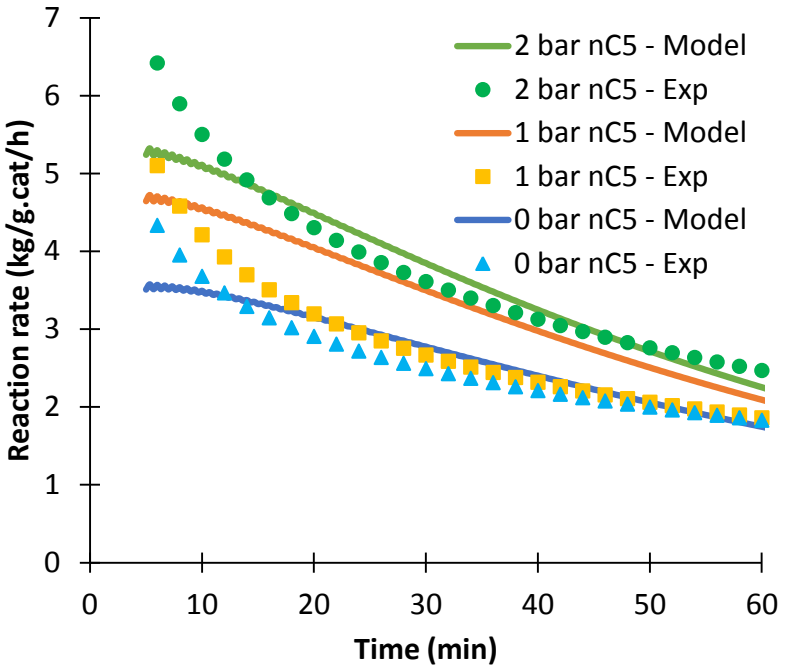

Figure 2. Polymerization rate calculated with the PFM and the experimental data, with 7 bar of ethylene, different amounts of n-pentane, and without hydrogen, at 80°C.

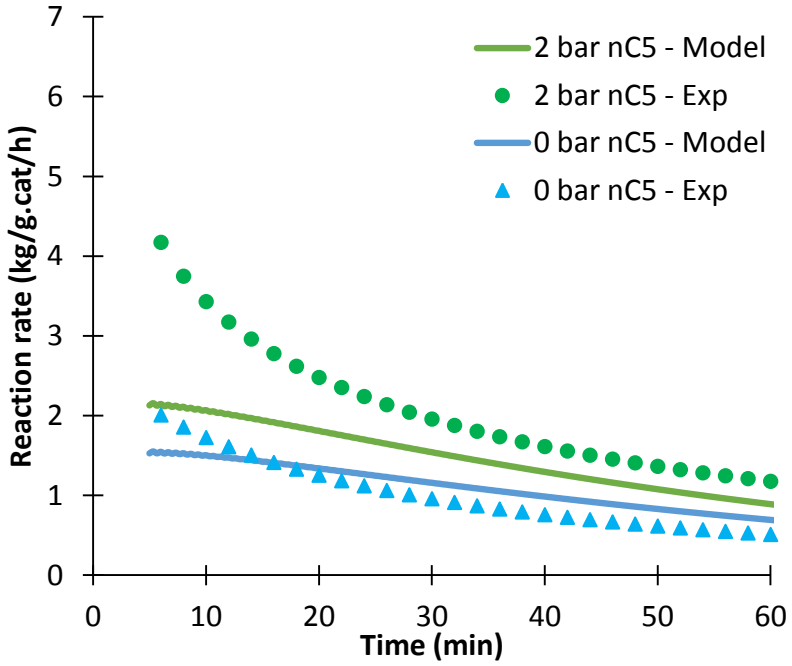

Figure 3. Polymerization rate calculated with the PFM and the experimental data, with 7 bar of ethylene, 3 bar of hydrogen and different amounts of n-pentane, at 80°C.

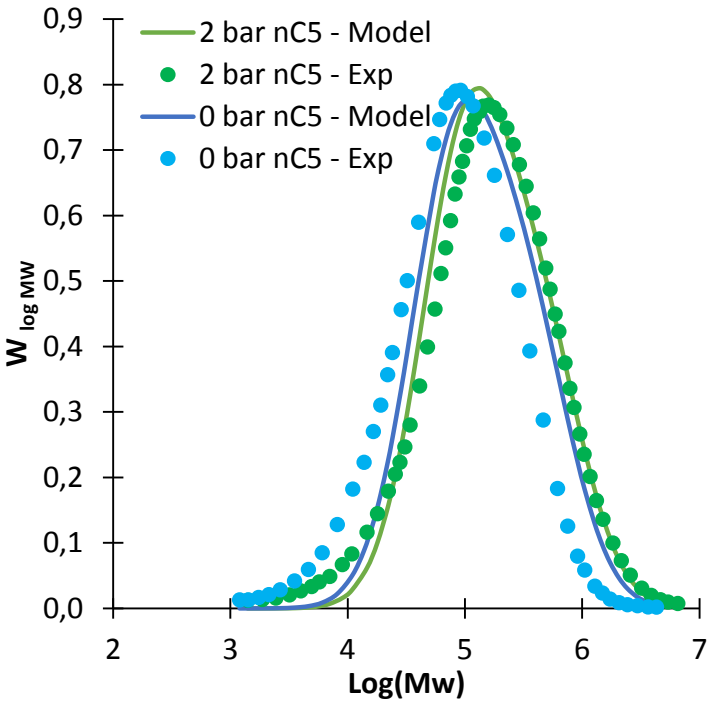

Figure 4. Molecular weight distribution calculated with the PFM and the experimental data measured with HT-GPC, with 7 bar of ethylene, 3 bar of hydrogen and different amounts of n-pentane at 80°C.

Results and discussion

Now that the single particle model has been validated, it can be used to explore the importance of the amount and type of ICA on the evolution of the concentration profiles, the reaction rate, the growth rate and the overheating of the polymer particle, as well as the molecular weight distribution of the polymer in different gas phase systems. The temperature and ethylene partial pressure were kept constant (i.e. 7 bar of ethylene and 80°C, respectively) and only the partial pressures of ICA and hydrogen are changing between each experiment $R_{\mathrm{p}i}$.

With the exception of a recent paper from Alizadeh et al.[22], virtually all single particle modelling studies appear to rely on binary solubility and diffusion models to describe ternary systems. However, it has been shown that the interactions between the two penetrants in ternary systems are crucial and lead to important changes when describing ethylene polymerization in gas phase. Adding ICA to the gas phase composition improves the heat capacity of the gas phase (so reduces changes in the particle temperature) but also increases

ethylene diffusion through the polymer phase which will lead to higher concentration of ethylene in the amorphous phase of the polymer. The instantaneous rate of ethylene polymerization is therefore higher in presence of ICA, as can be seen in Figure 5. The presence of ICA in the gas phase leads to a co-solubility effect of ICA on ethylene (and to an anti-solvent effect of ethylene on ICA) and to an enhanced diffusivity of ethylene. Accurate sorption and diffusion models are therefore important tools when modeling a single particle model in order to better analyze the influence of the gas phase composition on the polymerization rate.

Figure 5 compares the reaction rate as well as ethylene concentration gradients at 7 bar of ethylene, 1 bar of hydrogen and 1 (i.e. Rp8) or 2 (i.e. Rp9) bar of n-pentane. The binary model corresponds to the use of binary diffusivity and concentration of ethylene and n-pentane using SL EoS for binary systems, without taking into account the interactions between these two penetrants. The ternary corresponds to the use of ternary diffusivity and concentration of the gas phase mixture in the polymer, estimated by ternary Sanchez Lacombe EoS. It can be seen that using the binary thermodynamic model leads to an underestimation of the concentration of ethylene, leading to an underestimation of the polymerization rate. In the binary model, changing the concentration of ICA may only affect the temperature gradients inside the particle. However, the thermal effect was found to be negligible in this case, so no effect of the ICA is observed on the reaction rate when using the binary model.

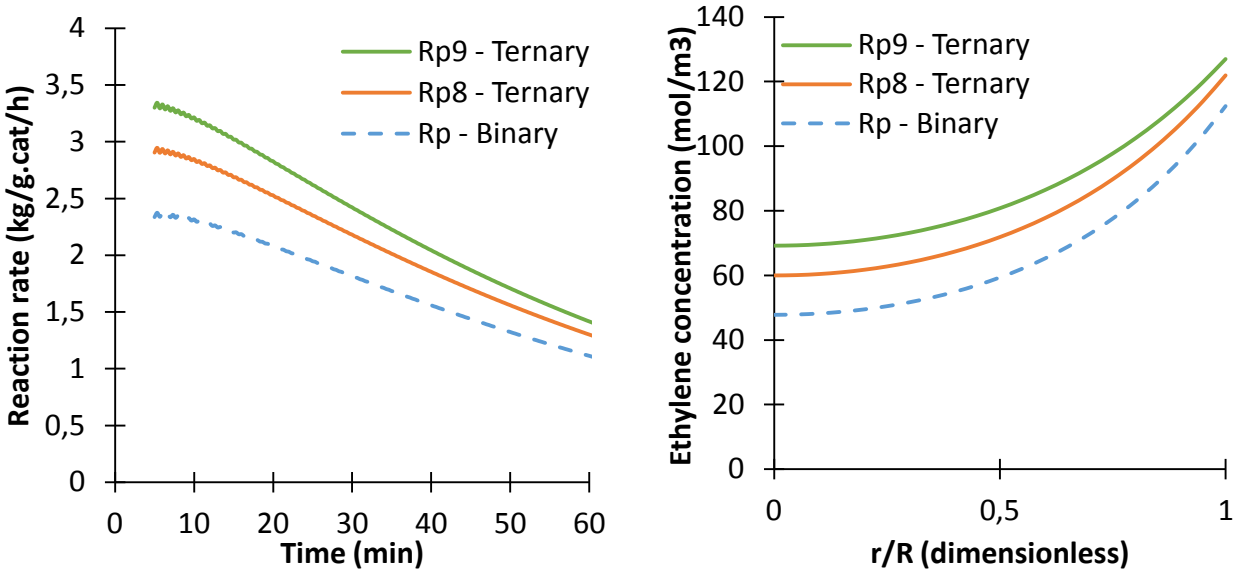

Figure 5. Effect of the thermodynamic model (i.e. binary, ternary) on the polymerization rate during the reaction and ethylene concentration gradients as a function of the normalized particle radius, with 7 bar C_2, for Rp_8:1 bar C_5, 1 bar H_2, and Rp_9: 2 bar C_5, 1 bar H_2. The concentrations are taken at 40 minutes of the reaction. The porosity is ε=0.05.

In the ternary model, note that the equilibrium concentration (i.e. the concentration of ethylene at the surface of the particle), is higher when ICA pressure is higher due to the co-solubility effect estimated by SL EoS. It is shown that the concentration of ethylene at the surface of the particle is about 122 mol m^{-3} with 1 bar of C_5 (i.e. Rp_8) and 127 mol m^{-3} with 2 bar of C_5 (i.e. Rp_9); so about a 4 % increase. A higher amount of ICA leads to a higher concentration of ethylene at the center of the particle, with an increase of 17 % with 1 bar of n-pentane, and of 31 % when 2 bars of n-pentane are used. This implies that the solubility increase alone cannot explain the observed effect of ICA on R_p, and that the co-diffusion effects are playing an important role too. Figure 6 shows that the diffusivity of ethylene in the ternary system doubles at 80°C when the n-pentane partial pressure passes from 0 (binary) to 2 bars. The diffusivities were calculated using Vrentas and Duda[24] correlation and its parameters are described in Table 4.

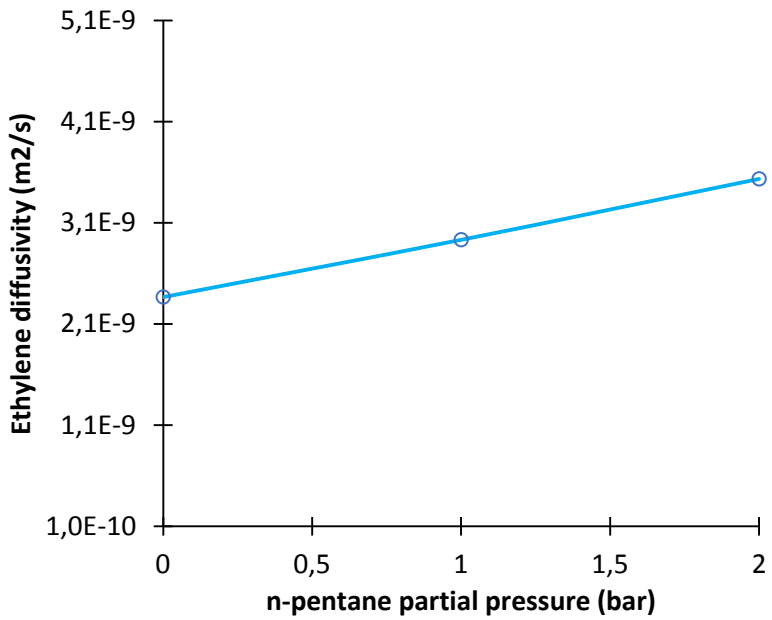

Figure 6. Ethylene diffusion coefficient in the binary ethylene/LLDPE system and in the ternary system in presence of 1 and 2 bar of n-pentane at 80°C.

These phenomena are clear in Figure 7, which shows ethylene concentration gradients inside the polymer particle for different ICA and hydrogen concentrations. Two consequences of ICA can be seen from this figure. First, as mentioned above, the concentration of ethylene at the surface of the particle will depend on the amount and type (see below) of the used ICA. Second, increasing the ICA partial pressure leads to less steep concentration gradients

(between the particle surface and its center) due to co-diffusion effects. Concerning the effect of hydrogen, increasing its partial pressure decreases the gradient of concentration of ethylene inside the growing polymer particle, with an increase of almost 66 % of ethylene concentration at the center of the particle when changing hydrogen from 0 to 3 bar, with 1 bar of n-pentane. This can be explained by the lower reaction rate when adding more hydrogen.

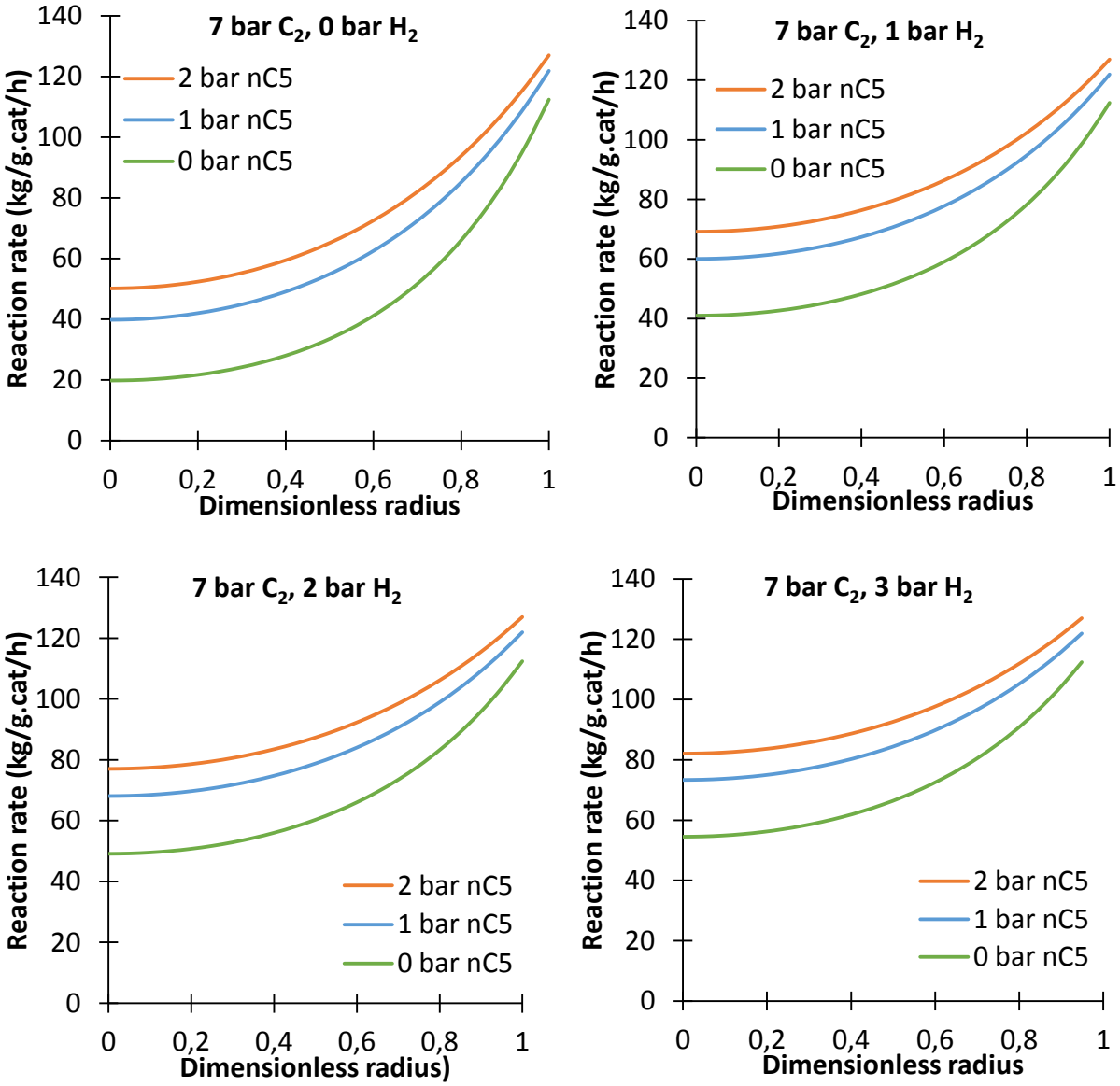

Figure 7. Ethylene concentration gradients as a function of the normalized particle radius at 40 minutes of the reaction for 7 bar of ethylene, 0-2 bar of n-pentane and 1-3 bar of hydrogen at 80°C.

The difference between the temperature of the particle surface T_s and the bulk temperature T_b describes the overheating of the particle. This parameter is shown in Figure 8 as a function of

the reaction time at the same conditions as previous simulations. We can see that the particle temperature rises significantly at the beginning of the reaction and then declines at 20 minutes to a steady-state value. This is expected as the reaction rate is higher at the beginning, and the surface area for heat exchange is the lowest. These temperature gradients were calculated using the Ranz-Marshall correlation which might overestimate the overheating, so it is possible that they are larger than might be the case in a fluidized bed reactor. Nevertheless, the relative changes between the different cases will be similar regardless of the chosen correlation. Regarding the effect of ICA, we can see that adding ICA leads to a slight increase of the boundary layer temperature gradient at the beginning of the polymerization, which is due to the higher monomer concentration in the particle and reaction rate. With the kinetic parameters chosen here, the increased heat capacity of the gas phase is outweighed by the increase in rate due to the addition of the ICA. On the other hand, as shown in Figure 2, Figure 3 and Figure 7, increasing the hydrogen partial pressure decreases the reaction rate which leads to a lower reaction rate.

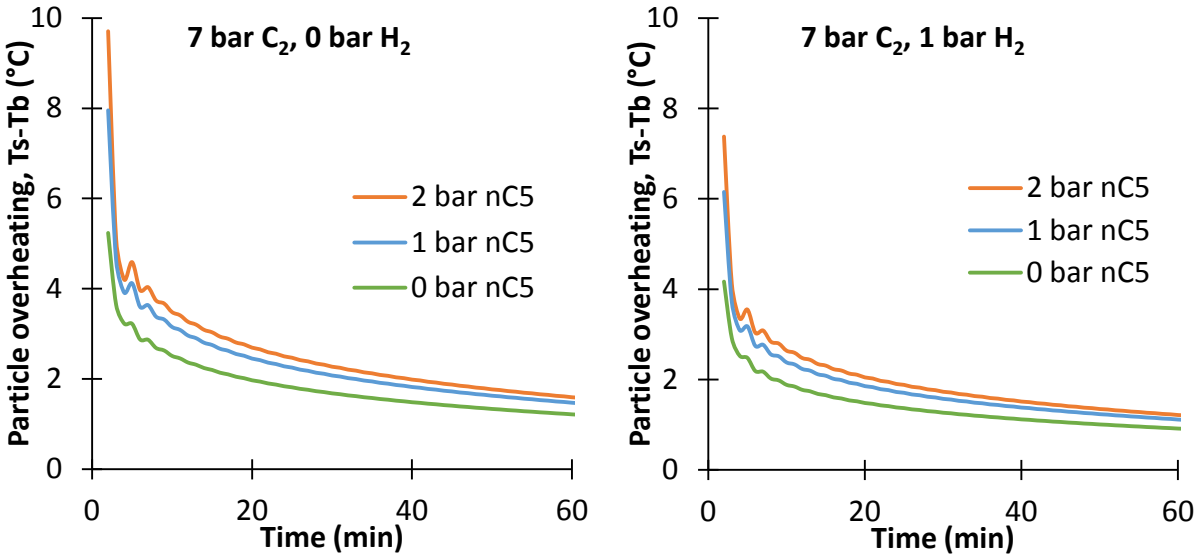

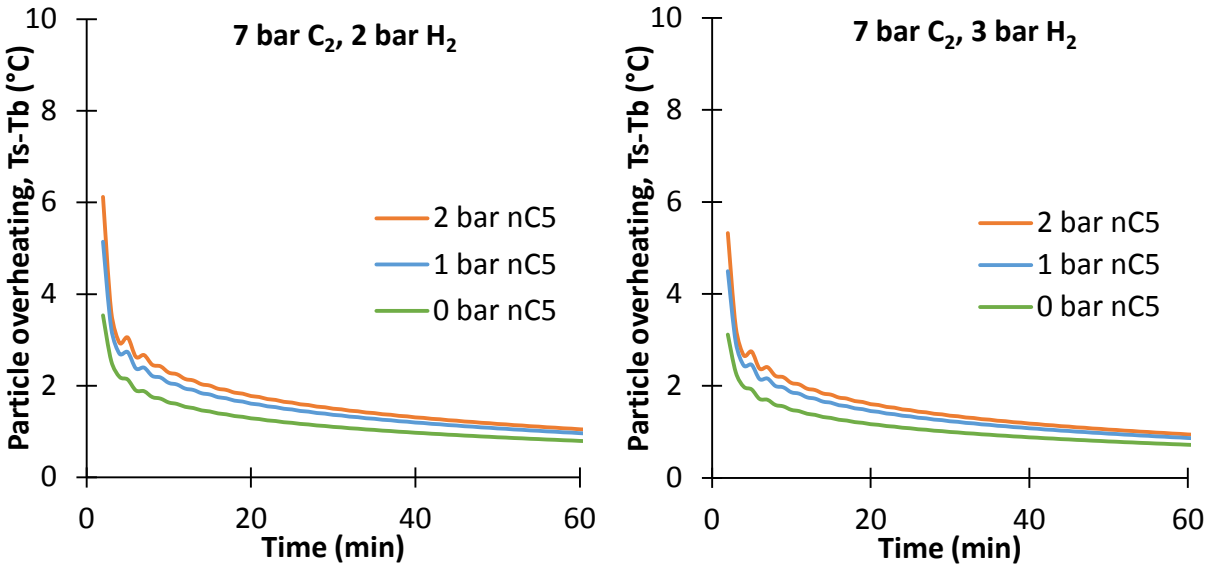

Figure 8. Particle overheating during ethylene polymerization 7 bar of ethylene, 0-2 bar of n-pentane and 1-3 bar of hydrogen at 80°C.

Figure 9 and Figure 10 show the effect of hydrogen and n-pentane partial pressure, respectively, on the molecular weight distribution. Hydrogen is the most important factor for controlling the MWD, because chain transfer to hydrogen is the main reaction producing dead polymer, even though the temperature as well as ethylene concentration may impact importantly the MWD. Increasing the hydrogen concentration leads to smaller molecular weight. However, increasing ICA partial pressure will lead to higher MW since it will increase the concentration of ethylene in the amorphous phase of the polymer, producing longer chains. The effect of ICA partial pressure is nevertheless less significant in the cases studied here than is the effect of hydrogen partial pressure on the MWD, as can be seen in Figure 10.

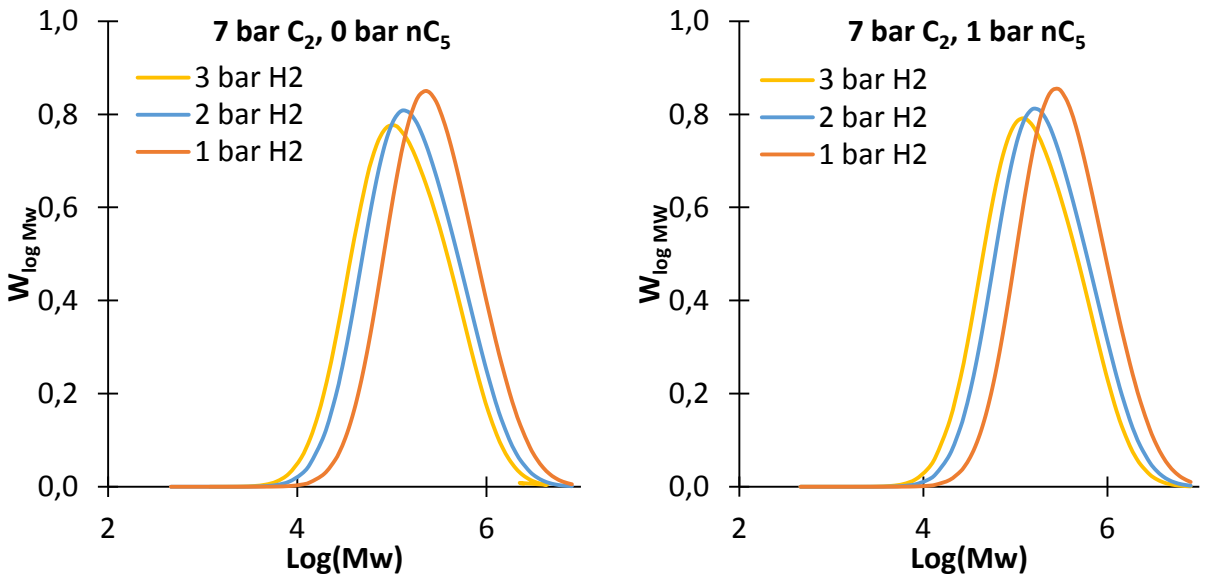

Figure 9. Effect of hydrogen on the molecular weight distribution calculated with the method of moments at 7 bar of ethylene and 0 and 1 bar of n-pentane at 80°C.

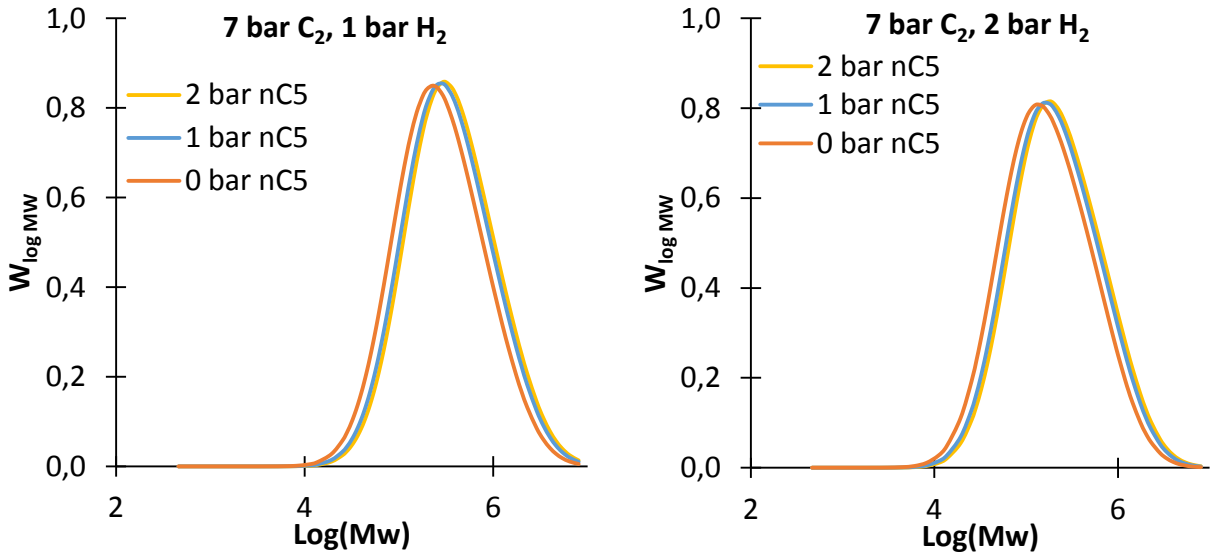

Figure 10. Effect of n-pentane on the molecular weight distribution calculated with the method of moments at 7 bar of ethylene and 1 and 2 bar of hydrogen, at 80°C.

As has been shown in previous papers[14,19,21], different ICA can influence the polymerization rate in different ways due to different co-solubility effects. One could therefore suspect that changing the ICA will lead to changes in the internal concentration gradients and MWD as well. To test this idea, simulations were run with the same kinetic parameters defined above, but with different parameters for the thermodynamic model (i.e. solubility and diffusivity). The SL parameters are given in

Table 2 and Table 3 and the Vrentas and Duda parameters for the diffusivity are given in Table 4 for both n-pentane and n-hexane at 80°C. The interaction parameters for the ethylene/n-hexane/HDPE system were taken from Alizadeh et al.[22] The simulation results are shown as normalized polymerization rates, normalized ethylene concentration gradient and normalized diffusivity to be able to quantify the change from the dry mode (pure ethylene) to the condensed mode in presence of n-hexane and n-pentane as ICAs.

Erreur ! Source du renvoi introuvable. compares the polymerization rate in presence of 7 bar of ethylene with either 1 bar of n-pentane or 1 bar of n-hexane normalized by the polymerization rate in dry mode (i.e. pure ethylene). It can be seen that the polymerization rate in presence of n-hexane is higher than in presence of an equivalent number of moles of n-pentane, and both are higher than ethylene alone. The increase in the polymerization rate is about 1.4 for n-pentane compared to 1.62 for n-hexane with respect to the one with pure ethylene. This trend was validated with Alizadeh et al.[18] who found out that the increase in the polymerization rate in presence of 1 bar of n-pentane was about 1.5 and in presence of 0.8 bar n-hexane about 1.85. They found a higher effect in presence of n-hexane than this work because their crystallinity was lower than the one used in the present study. It is also interesting to note that the slopes of the curves are different, showing that there are also diffusion effects involved, and that the higher diffusion coefficients for n-pentane and for n-hexane lead to faster rates at the beginning of the polymerization.

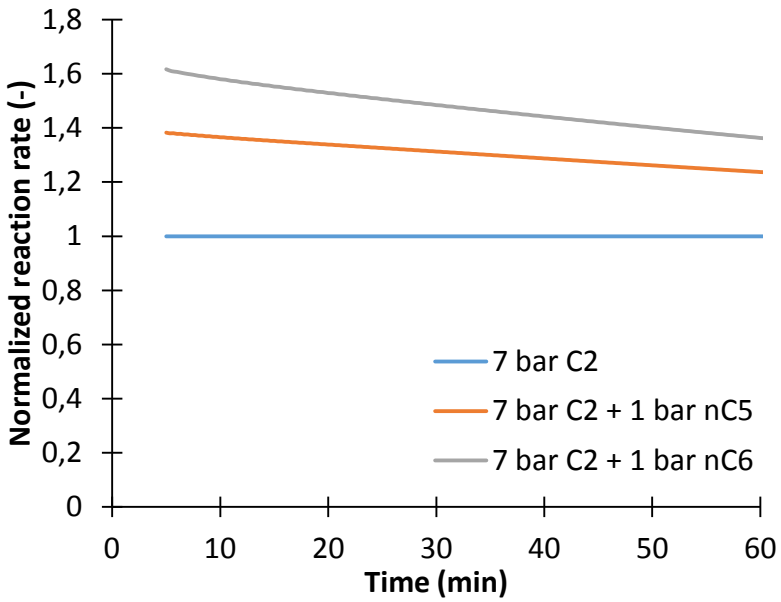

Figure 11.Polymerization rate for 7 bar of ethylene at 80°C with 1 bar of n-pentane and n-hexane normalized by the polymerization rate without ICA.

The co-solubility and co-diffusivity effects can be clearly seen in Figures 12 and Figure 13. Figure 12 shows the diffusivity of ethylene in the ternary system of ethylene/ICA/PE normalized by the diffusivity of ethylene in the binary system, with n-pentane or n-hexane as ICA. It is shown that adding 1 bar of n-hexane leads to a higher increase of ethylene diffusivity with respect to 1 bar of n-pentane. Indeed, the heavier the ICA is, the higher the diffusivity will be. Figure 13 shows ethylene concentration gradient at 40 minutes of the reaction with either 1 bar of n-pentane or 1 bar of n-hexane normalized by the concentration gradient of ethylene in dry mode as a function of the normalized particle radius. It is shown that the equilibrium concentration calculated from SL EoS is slightly higher in the presence of n-hexane than n-pentane. The difference is expected to be higher, but the crystallinity of LLDPE in presence of n-hexane is about 60 % compared to 45 % in presence of n-pentane. So, it is demonstrated the concentration of ethylene at the surface is function of ethylene pressure but also on the type and amount of ICA used during the polymerization reaction. Besides, it is shown that adding ICA leads to higher concentration gradients of ethylene inside the polymer particle due to the co-solubility effect of ICA increasing ethylene concentration in the amorphous phase of the polymer. Furthermore, a heavier ICA leads to a higher concentration gradient of ethylene due to the co-diffusion effect of ICA increasing the diffusivity of ethylene through the growing polymer particle.

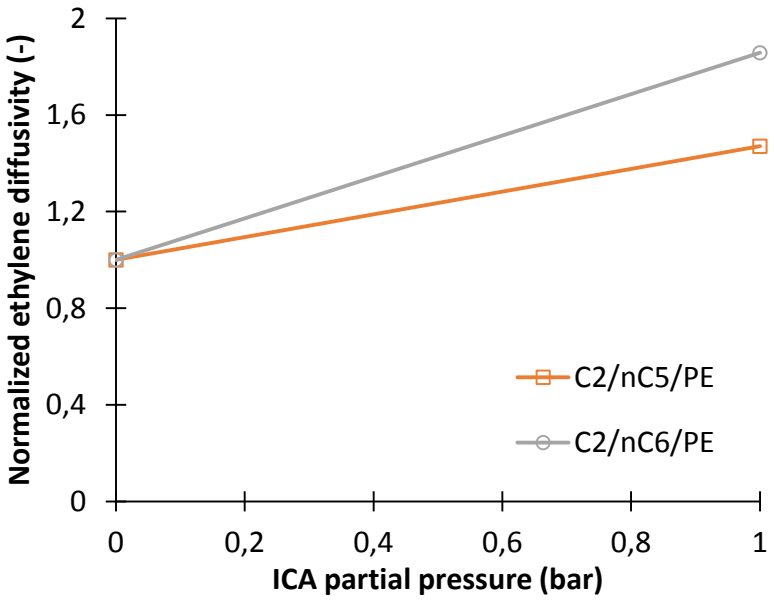

Figure 12. Ethylene diffusivity in the ternary system of ethylene/ICA/PE normalized by ethylene diffusivity in the binary system of ethylene/PE as a function of ICA partial pressure at 80°C.

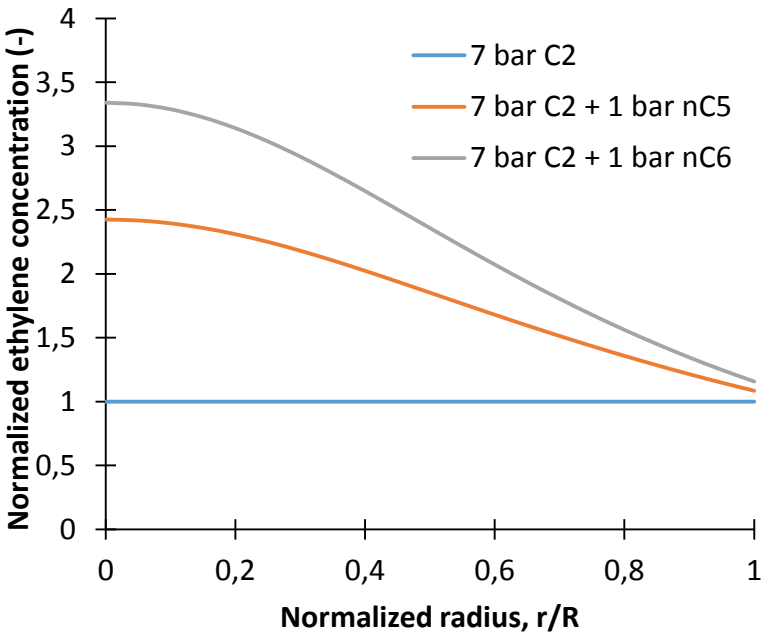

Figure 13. Ethylene concentration gradient in the particle at 40 minutes of the reaction for 7 bar of ethylene at 80°C with 1 bar of n-pentane and n-hexane normalized by ethylene concentration gradient without ICA.

Conclusion

A single particle model, based on the RPPFM has been developed in this paper in order to describe the polymerization of ethylene in presence of n-pentane and hydrogen at 80°C. The model was adapted to quantify the impact of the gas phase composition (i.e. monomer, n-pentane, hydrogen) on the reaction rate, the concentration and temperature gradients and the molecular weight distribution. 0-2 bar of n-pentane have been used, and 0-3 bar of hydrogen, with a constant pressure of 7 bar of ethylene. The particle model was validated with experimental reaction rate data and the molecular weight distribution through the HT-GPC.

The importance of using an accurate thermodynamic model describing both the equilibrium concentration of the different penetrants as well as the diffusion of these penetrants in the amorphous phase of the polymer has been highlighted. The Sanchez-Lacombe EoS has been used as sorption model, and Vrentas and Duda as diffusion model. It is important to note that the concentration of hydrogen being very low compared to ethylene concentration in the polymer, it was considered constant over time and the particle radius, and not influencing the concentration/diffusivity of ethylene. Model predictions showed that the use of binary models leads to an underestimation of ethylene concentration in the particle and therefore of the polymerization rate, because of the co-solubility and co-diffusion effects. The developed

model was evaluated under different operating conditions with of different types of ICAs (i.e. n-pentane, n-hexane) and it demonstrated that accurate thermodynamic models were crucial when describing their effects on the polymerization reaction.

The effect of the gas phase composition has been evaluated through the polymerization rate, ethylene concentration gradients inside the polymer particle, the growth and overheating of the polymer particle, and finally the molecular weight distribution. In all the results, the higher the partial pressure of hydrogen is, the lower is the productivity and the molecular weight of the polymer, whereas increasing n-pentane (or n-hexane) partial pressure increases the productivity and the polymer molecular weight.

Acknowledgments

The authors would like to acknowledge the financial support of the Agence Nationale de la Recherche (ANR) for Project Thermopoly ANR-16-CE93-0001. The authors would also like to thank ETH Zurich, and especially Dr. Tommaso Casalini and Prof. Giuseppe Storti for their help with the validation of the Single Particle Model with n-hexane as ICA. The authors would also like to thank Mr. Niyi Ishola for performing certain polymerization experiments.

References

1. T.F.L. McKenna, *Macromol. Symp.*, **2007**, *260*, 65.
2. T.F.L. McKenna, A. Di Martino, G. Weickert, J.B.P. Soares, *Macromol. React. Eng.*, **2010**, *4*, 40.
3. R. van Grieken, A. Carrero, I. Suarez, B. Paredes, *Macromol. Symp.*,**2007**, *259*, 243.
4. D.A. Estenoz, M.G. Chiovetta, *Polym. Eng. Sci.*,**1996**, *36*, 2229.
5. A. Alizadeh, T.F.L. McKenna, *Macromol. React. Eng.*, **2018**, *12*, 1700027.
6. J.A. Debling, W.H. Ray, *Ind. Eng. Chem. Res.*, **1995**, *34*, 3466.
7. R.A. Hutchinson, C.M. Chen, W.H. Ray,. *J. Appl. Polym. Sci.*, **1992**, *44*, 1389.
8. H. Hatzantonis, H. Yiannoulakis, A. Yiagopoulos, C. Kiparissides, *Chem. Eng. Sci.*, **2000**, *55*, 3537.

9. J.B.P. Soares, T.F.L. McKenna, Polyolefin Microstructural Modeling. 187-269, Chapter 6 in 1Polyolefin Reaction Engineering (Wiley-VCH Verlag GmbH & Co. KGaA, 2012).
10. T.F.L. McKenna, M.A. Bashir, Fragmentation, Particle Growth and Single Particle Modelling., Chapter 5 in *Multimodal Polymers with Supported Catalysts: Design and Production* (eds. Albunia, A. R., Prades, F. & Jeremic, D.) 81–114 (Springer International Publishing, 2019).
11. T.F. McKenna, J.B.P. Soares, *Chem. Eng. Sci.*,**2001**, *56*, 3931.
12. V. Kanellopoulos, G. Dompazis, B. Gustafsson, C. Kiparissides, *Ind. Eng. Chem. Res.*, **2004**, *43*, 5166.
13. T.F.L. McKenna, *Macromol. Reacn. Eng.*, **2019**, *13*, 1800026 (2019).
14. M. Namkajorn, A. Alizadeh, E. Somsook,T.F.L. McKenna, *Macromol. Chem. Phys*.; **2014**, *215*, 873.
15. J.M. Jenkins III, R.L. Jones, T.M. Jones, EP 0241947B1, **1987**.
16. J.M. Jenkins III, R.L. Jones, T.M. Jones, US Patent 4543399 (both to Union Carbide Chemical and Plastics Technology Company), **1985**.
17. A. Alizadeh, M. Namkajorn, E. Somsook, T.F.L. McKenna, *Macromol. Chem. Phys.*, **2015**, *216*, 903.
18. A. Alizadeh, M. Namkajorn, E. Somsook, T.F.L. McKenna, *Macromol. Chem. Phys*., **2015**, 216, 985.
19. M. Namkajorn, A. Alizadeh, D. Romano, S. Rastogi, T.F.L. McKenna, *Macromol. Chem. Phys.*, **2016**, *217*, 1521.
20. F.N. Andrade, T.F.L. McKenna, *Macromol Chem Phys*., **2017**, 1700248,.
21. N. Ishola, F.N. Andrade, F. Machado, T.F.L. McKenna, *Macromol. React. Eng*., **2020**, 2000021

22. A. Alizadeh, F. Sharif, M. Ebrahimi, T.F.L. McKenna, *Ind. Eng. Chem. Res.,***2018**, *57*, 6097
23. J.S. Vrentas, J.J. Duda, J. L., H.C. Ling, *J. Memb. Sci.*, **1989**, *40*, 101.
24. J.S. Vrentas, J.J. Duda, J. L., H.C. Ling, *J. Polym. Sci. Polym. Phys. Ed.*, **1984**, *22*, 459.
25. V. Kanellopoulos, E. Tsiliopoulou, G. Dompazis, V. Touloupides, C. Kiparissides, *Ind. Eng. Chem. Res.*, ***2007***, *46*, 1928.
26. M.A. Bashir, V. Kanellopoulos, M. Al- haj Ali, T.F.L. McKenna, *Macromol. React. Eng.*, **2020,** *14*, 1900029.
27. G. Weickert, G.B. Meier, J.T. Pater, K.R. Westerterp, *Chem. Eng. Sci.*, **1999**, *54*, 3291.
28. T.F. McKenna, J. Dupuy, JR. Spitz, *J. Appl. Polym. Sci.*, **1995**, *57*, 371.
29. I.C. Sanchez, R.H. Lacombe, *J. Polym. Sci. B Polym. Lett. Ed.*, **1977**, *15*, 77.
30. A. Alizadeh, J. Chmelař, F. Sharif, M. Ebrahimi, J. Kosek, T.F.L. McKenna, *Ind. Eng. Chem. Res.*, **2017**, *56*, 1168.
31. A. Alizadeh, Study of sorption, heat and mass transfer during condensed mode operation of gas phase ethylene polymerization on supported catalyst. Ph.D. Thesis, Departement of Chemical Engineering, Queen's University, Kingston, ON, Canada, 2014.
32. R.F. Alves, T..L. McKenna, *Chem. Eng. J.*, **2020**, *383*, 123114.
33. W. Yao, X. Hu, Y. Yang, *J. Appl. Polym. Sci.*, **2007**, *104*, 3654).
34. W. Yao, X. Hu, Y. Yang, *J. Appl. Polym. Sci.*, **2007**, *103*, 1737.
35. J. Sun, H. Wang, M. Chen, J. Ye, B. Jiang, J. Wang, Y. Yang, C. Ren, *J. Appl. Polym. Sci.*, **2017**, *134*, 44507.
36. N. Wakao, J.M. Smith, *Ind. Eng. Chem. Fund.*, **1964**, *3*, 123.
37. A. Yiagopoulos, H. Yiannoulakis, V. Dimos, C. Kiparissides, *Chemical Engineering Science*, **2001**, *56*, 3979.
38. J.M. Zielinski, J.J Duda, *AIChE J.*, **1992**, *38*, 405.

39. J.S. Vrentas, J.J. Duda, J. L., H.C. Ling, A.C. Hou, *J. Polym. Sci. Polym. Phys. Ed.*, **1984**, *23*, 289.
40. A. Gonzalez, S. Eceolaza, A. Etxeberria, J.J. Iruin, *Journal of Applied Polymer Science*, **2007**, *104*, 3871.
41. V. Kanellopoulos, D. Mouratides, E. Tsiliopoulou, C. Kiparissides, *Macromolecular Reaction Engineering*, **2007**, *1*, 106.
42. Soares, J., McKenna, T.FL., Polyolefin Reaction Engineering., Chapter 6 in (Wiley-VCH Verlag GmbH & Co. KGaA, 2012). doi:10.1002/9783527646944.ch6.
43. F.N. Andrade, T.F.L. McKenna, *Macromol Chem Phys*., **2017**, 1700248.
44. C. Chatzidoukas, J.D. Perkins, A.N. Pistikopoulos, C Kiparissides, *Chemical Engineering Science*,**2003**, *58*, 3643
45. N.M. Ghasem, W.L. Ang, M.A. Hussain, *Korean J. Chem. Eng*., **2009**, *26*, 603
46. K.B. McAuley, J.F. MacGregor, A.E. Hamielec, *AIChE Journa*, **1990,** *36*, 837.